When Classical Trajectories Get to Quantum Accuracy: The Scattering of H 2 on Pd(111)

A. Rodríguez-Fernández, L. Bonnet, C. Crespos, P. Larrégaray, R. Díez Muiño

When Classical Trajectories Get to Quantum Accuracy: the Scattering of H_2 on Pd(111)

A. Rodríguez–Fernández,[†,‡] L. Bonnet,[*,†,¶] C. Crespos,[†,¶] P. Larregaray,[†,¶] and R. Díez Muiño[§,‡]

†*Université de Bordeaux, ISM, UMR 5255, F-33400 Talence, France*

‡*Centro de Física de Materiales CFM/MPC (CSIC-UPV/EHU), Paseo Manuel de Lardizabal 5, 20018 Donostia-San Sebastián, Spain*

¶*CNRS, ISM, UMR5255, F-33400 Talence, France.*

§*Donostia International Physics Center (DIPC), Paseo Manuel de Lardizabal 4, 20018 Donostia-San Sebastián, Spain*

E-mail: claude-laurent.bonnet@u-bordeaux.fr

Abstract

When elementary reactive processes occur at so low energies that only few states of reactants and/or products are available, quantum effects strongly manifest and the standard description of the dynamics within the classical framework fails. We show here, for H_2 scattering on Pd(111), that by pseudo-quantizing in Bohr's spirit the relevant final actions of the system, along with adequately treating the diffraction-mediated-trapping of the incoming wave, classical simulations get to an unprecedented and spectacular agreement with state-of-the-art quantum dynamics calculations.

Graphical TOC Entry

Keywords

Completar

Introduction

In the last five decades, synergetic advances in theory and experiments associated with a tremendous increase of computing power, have allowed a detailed understanding of the reaction dynamics of chemical elementary processes.[1–10] For chemical reactions involving a small number of degrees-of-freedom (DOF) (typically less than or equal to 6), quantum dynamics calculations might be now regarded as exact since they generally provide results in excellent agreement with experiments.[11,12] However, reaction dynamics studies focus on systems of ever increasing size[13–28] for which the quasi-classical trajectory (QCT) method is at this time the only practical tool to apply. A crucial issue is thus to develop theoretically justified corrections to carry out classical dynamics studies of chemical reactions in a quantum spirit.[29] Obviously, these approximations must be validated on small systems for which benchmark quantum dynamics calculations are available. The development and test of such corrections is the central focus of this work (only processes taking place on a single electronic state and involving negligible tunneling are considered in the following).

Gaussian binning (GB)[16,29–31] and the *adiabaticity correction* (AC)[32] have been proposed some years ago in order to account for product vibrational quantization, and classical overweighting of adiabatic non-reactive collisions, respectively. These corrections, both supported by semiclassical arguments,[29,33] were recently shown[29,33,34] to significantly improve the capability of the QCT method to describe gas-phase and gas-surface *barrierless reactions in the quantum regime*, where only a few internal states are available to the reactants and/or products.

To date, GB has only been applied to the vibrational motions of final products. The originality of the present work is that, for the first time, GB is applied to nearly all product quantized motions of a relatively complex collisional problem, the scattering of H_2 on Pd(111).[1,35–37] These full GB calculations, combined with the AC correction, are shown to amazingly reproduce benchmark quantum time-dependent wave-packet (Q-TDWP) results at low collision energies for which the standard QCT method completely fails.[1,35–37] This

specific system is here chosen because dissociative adsorption, inelastic scattering as well as surface diffraction have been intensively scrutinized both theoretically and experimentally over the last two decades.[1,35–39]

Section 2 details the implementation of our methodology. Section 3 discusses the comparison of its results with Q-TDWP calculations. Section 4 concludes.

Theoretical Methodology

In this work, we assume that H_2 impinges the surface at normal incidence in the rovibrational ground state ($v = 0, j = 0$) with the collision energy E_i. H_2 may either stick on the palladium surface, or bounce back to the vacuum. E_i will be small enough for the first excited vibrational state of H_2 to be unavailable after rebound. The quantum probability of the sticking event, resulting from Q-TDWP calculations[40] on a Density-Functional-Theory-based ground state potential energy surface,[41,42] is displayed in Fig. 1 (black squares). Within the classical picture, rebound may lead to a final vibrational energy of H_2 lower than its zero point energy (ZPE) and this is all the more probable when the initial collision energy is much smaller than the ZPE. In such a case, the classical sticking probability artificially falls down with respect to the quantum value. This is clearly seen in Fig. 1 (blue circles) for collision energies lower than 50 meV (some details on the QCT calculations are given later below).

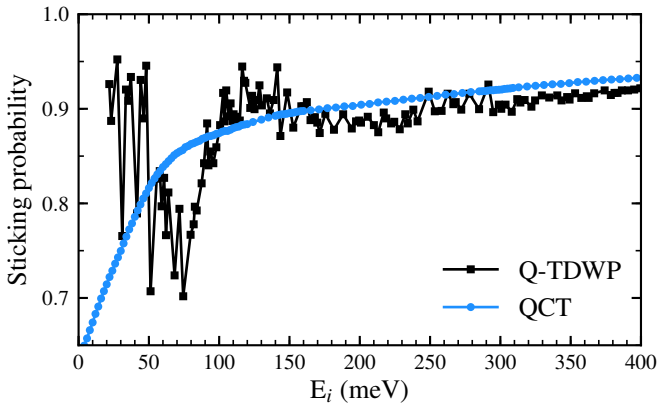

Figure 1: Quantum (black squares) and classical (blue circles) sticking probabilities for $H_2(0,0)$ + Pd(111) as a function of the collision energy.

Recently, however, we remedied this issue by taking into account Bohr's condition of quantization in the analysis of trajectory results.[33] Transposed to molecular systems, Bohr's idea is that a quantum transition can be classically described provided that one only retains those classical paths connecting integer actions of the molecular system before the transition, with integer actions after the transition (actions are the classical analogs of quantum numbers).[43] So far, we have only considered the vibrational action of H_2, which is enough for qualitatively recovering the non-monotonous behaviour of the sticking probability.[33] In this work, however, we show that accounting for (nearly) all the actions of the problem (detailed further below) leads to a drastic improvement of the predictions, not only for the sticking probability, but also for the distribution of the final quantum states of the system after reflection.

However, action quantization is not the only effect which must be taken into account in the classical trajectory approach. As a matter of fact, the title reaction involves in part trapped trajectories[41] along which H_2 wanders about the paladium surface before returning back to the vacuum or fragmenting (then leading to sticking), and in part trajectories involving a single rebound against repulsive walls before reflecting back. Among the latter, several bounce back against nearly isotropic parts of the walls, in such a way that the internal motion of H_2 evolves adiabatically throughout the whole collision. Semiclassical developments show that the quantum counterpart of these adiabatic (or elastic) paths is the diffraction of the incident wave.[33] Since H_2 is on average attracted by the palladium surface, and diffraction excites the rotational motion of H_2 to the detriment of its recoil motion with respect to the surface, the diffracted wave is expected to get trapped and eventually contribute to both sticking and inelastic bouncing, just as the rest of the incident wave. The classical transposition of this scenario of diffraction-mediated-trapping is that the probability carried by adiabatic paths is redistributed to the remaining paths.[33] For simplicity's sake, we shall assume that the redistribution is democratic, which amounts to ignore adiabatic paths and renormalize to unity the probability carried by the remaining trajectories. The results of the

present article show that the combination of this adiabaticity correction (AC) and Gaussian binning lead to a remarkable description of the dynamics at low energies.[32–34]

Besides, we have found no other quantum effect playing a significant role in the title reaction. In the remainder of this section we consider the practical implementation of the previous ideas.

Practical application of Bohr's condition of quantization: Gaussian binning

Actions

The vibrational action x,[43] rotational action J and diffractive actions (a_n, a_m) that we shall be considering at the end of each non reactive trajectory, are given by

$$x = \frac{1}{2\pi} \oint p dr - \frac{1}{2}, \tag{1}$$

$$J = \frac{-1 + \sqrt{1 + 4L_f^2}}{2}, \tag{2}$$

$$a_n = \frac{\Delta}{2\pi} P_X^f \tag{3}$$

and

$$a_m = \frac{\Delta}{4\pi} \left(P_X^f + \sqrt{3} P_Y^f \right). \tag{4}$$

We work in $\hbar$ unit throughout this work. r is the H_2 bond length and p its conjugate momentum. The cyclic integral in Eq. 1 is calculated by running each trajectory over one vibrational period once H_2 has reached the vacuum, i.e., no longer interacts with the surface. L_f is the modulus of the final classical rotational angular momentum $\boldsymbol{L}_f$ of H_2. Eq. 2 is deduced by equating L_f^2 and $J(J+1)$. P_X^f and P_Y^f are the projections of the final linear momentum vector of H_2 on the X and Y axis of Pd(111), chosen in such a way that ($X =$

$0, Y = 0)$ and $(X = \Delta = 2.75$ Å$, Y = 0)$ are the positions of two nearest neighbour surface atoms. The Z axis is normal to the surface. a_n and a_m are the classical analogs of Miller indices n and m. More details on these diffractive actions can be found in the supporting information.

The fifth action of the problem is the projection J_Z of $\boldsymbol{J}$ on the Z axis orthogonal to the surface, where $\boldsymbol{J}$ is the vector of modulus J parallel to $\boldsymbol{L}_f$. Contrary to (x, J, a_n, a_m), however, this action is not involved in the quantization of energy partitioning (see further below). Since GB aims at best selecting those trajectories complying with this quantization, and J_z is of no use for this purpose, we ignore it from now on.

We call $\mathbf{a}$ and $\bar{\mathbf{a}}$ the quadruplets (x, J, a_n, a_m) and $(\bar{x}, \bar{J}, \bar{a}_n, \bar{a}_m)$, respectively, where $\bar{q}$ is the nearest integer of q. In the following, we assume that $\mathbf{a}$ contributes to no other quantum state than $\bar{\mathbf{a}}$.

Energies

At the end of a given non reactive trajectory, the total energy E satisfies

$$E = \frac{P_Z^2}{2M} + E(\mathbf{a}) \tag{5}$$

with

$$E(\mathbf{a}) = E_{rovib}(x, J) + E_{\parallel}(a_n, a_m), \tag{6}$$

$$E_{rovib}(x, J) = \frac{p^2}{2\mu} + V(r) + \frac{L_f^2}{2\mu r^2} \tag{7}$$

and

$$E_{\parallel}(a_n, a_m) = \frac{8\pi^2}{3M\Delta^2}\left(a_n^2 + a_m^2 - a_n a_m\right). \tag{8}$$

M and μ are the total and reduced masses of H_2, respectively. $P_Z^2/(2M)$ is the energy of recoil along the Z-axis. $E_{rovib}(x, J)$ is the rovibrational energy of H_2 ($V(r)$ being its potential

energy in the vacuum). $E_{\parallel}(a_n, a_m)$ is the energy in the translational motion parallel to the surface, obtained from its definition in Cartesian coordinates and Eqs. 3 and 4. $E(\mathbf{a})$ is thus the energy in the degrees-of-freedom submitted to spatial constraints (bound space, surface periodicity), thus involving a discrete spectrum in quantum mechanics. The energy of quantum state $\bar{\mathbf{a}}$, closest to $\mathbf{a}$, is given by

$$E(\bar{\mathbf{a}}) = E_{rovib}(\bar{x}, \bar{J}) + E_{\parallel}(\bar{a_n}, \bar{a_m}). \tag{9}$$

$E_{rovib}(\bar{x}, \bar{J})$ is calculated as follows: p, in Eq. 1, is replaced by

$$p = \pm \left[2\mu \left(E_{trial} - \frac{\bar{J}(\bar{J}+1)}{2\mu r^2} - V(r) \right) \right]^{1/2} \tag{10}$$

where E_{trial} is initially taken at the bottom of the well of the effective potential $V(r) + \bar{J}(\bar{J}+1)/(2\mu r^2)$. The corresponding value of x is thus -1/2. E_{trial} is then increased until $x = \bar{x}$ (to the required accuracy), and $E_{rovib}(\bar{x}, \bar{J})$ is identified as the last value of E_{trial}. The dependence of $E_{rovib}(\bar{x}, \bar{J})$ on $\bar{x}$ and $\bar{J}$ clearly appears in the previous reasoning. Analogously, $E_{rovib}(x, J)$ is fully specified by x and J (although this is not explicit on the right-hand-side of Eq. 7).

Standard binning: SB

In this traditional approach,[44] trajectories are usually assigned unit statistical weight. This is what we shall assume for sticking trajectories. On the other hand, for non reactive trajectories, the final value of j can only be even since the initial value of j is 0 (parity conservation). Therefore, these trajectories are assigned the weight

$$w_{SB}(\mathbf{a}) = 2(1 + \delta_{\bar{J}0}) \tag{11}$$

if $\bar{J}$ is even, and 0 if $\bar{J}$ is odd. The Kronecker delta takes into account the fact that for $\bar{J} = 0$, J belongs to the range [0,0.5] whereas for $\bar{J} \geq 2$, J belongs to the range $[\bar{J} - 0.5, \bar{J} + 0.5]$. The blue circles in Fig. 2 were obtained by means of this approach.

Action-based Gaussian binning: GB

Within the Gaussian Binning procedure,[30] the statistical weight differs for each trajectory depending on the values of the final actions. Consider the statistical weight

$$w_{GB}(\mathbf{a}) = G(x)G(J)G(a_n)G(a_m)w_{SB}(\mathbf{a}) \tag{12}$$

with

$$G(q) = \frac{1}{\sqrt{\pi}\epsilon} exp\left[-\left(\frac{q-\bar{q}}{\epsilon}\right)^2\right]. \tag{13}$$

Bohr's condition of quantization would exactly be realized if ϵ would tend to an infinitely small (positive) value. In such a case, one would indeed have $G(q) = \delta(q-\bar{q})$, and only those trajectories leading to integer actions would contribute to the process. This is, however, only of formal interest. In practice, one must increase the value of ϵ until $w_{GB}(\mathbf{a})$ takes a significant value for at least $\sim 10^2$ trajectories. The normalization of $w_{GB}(\mathbf{a})$ is identical to that of $w_{SB}(\mathbf{a})$, i.e., for ϵ small enough, integrating $w_{GB}(\mathbf{a})$ over the unit cube of the action space centered at $\bar{\mathbf{a}}$ leads to unity.

Energy-based Gaussian binning: 1GB

Instead of pseudo-quantizing the four actions by means of four Gaussians, the alternative is to pseudo-quantize $E(\mathbf{a})$ by means of a single Gaussian.[16,45] Formally, trajectories are thus assigned the statistical weight

$$w_{1GB}(\mathbf{a}) = \frac{1}{\sqrt{\pi}\epsilon} e^{-\left[\frac{E(\mathbf{a})-E(\bar{\mathbf{a}})}{2\epsilon E(\mathbf{0})}\right]^2} w_{SB}(\mathbf{a}), \tag{14}$$

where $E(\mathbf{0})$ is the harmonic zero-point vibrational energy. Eq. 14 is a straightforward application of Eq. (13) of Ref.[16] $w_{1GB}(\mathbf{a})$ clearly puts strong emphasis on those trajectories leading to $E(\mathbf{a})$ close to $E(\bar{\mathbf{a}})$. As previously, ϵ is increased until $w_{1GB}(\mathbf{a})$ takes a significant value for at least $\sim 10^2$ trajectories. For a statistical (i.e., uniform) distribution of $\mathbf{a}$, it was analytically proved that GB and 1GB lead to rigorously identical results.[45] Moreover, recent simulations confirmed the similarity of GB and 1GB predictions for non statistical processes.[9]

We have numerically checked that the normalization of $w_{1GB}(\mathbf{a})$ is identical to that of $w_{SB}(\mathbf{a})$ (again, for ϵ small enough). However, this is generally not so, and numerically renormalizing $w_{1GB}(\mathbf{a})$ according to $w_{SB}(\mathbf{a})$ is a prerequisite for a safe use of the 1GB procedure.

Practical detection of adiabatic paths

As seen before, adiabatic paths involve a single rebound against weakly anisotropic repulsive walls before reflecting back to the vacuum with nearly no perturbation of the internal motion of H_2. In practice, we have found that trajectories involving a single rebound spend less than 100 fs at a distance from the surface lower than 3 Å. We have thus defined adiabatic paths by the trajectories complying with the previous criterion, and leading to the final vibrational action x within the narrow range [-0.02,0.02], centered at the initial value of x. We have checked that the width of this window does not affect the results as long as it is kept much smaller than 1, the action spacing between two neighboring vibrational states.

Sticking and rebound probabilities

When the AC correction is not taken into account, the sticking probability is given by:

$$P_S^X = \frac{N_S}{N_S + \Sigma_R^X(\mathbf{a})} \tag{15}$$

with

$$\Sigma_R^X(\mathbf{a}) = \sum_{k=1}^{N-N_S} w_X(\mathbf{a}). \tag{16}$$

X stands for SB, GB or 1GB, according to the procedure employed to calculate the weights. N is the total number of trajectories, N_S the number of trajectories leading to sticking and $\Sigma_R^X(\mathbf{a})$ is the total weight of the $N - N_S$ nonreactive trajectories.

Analogously, the probability of reflection in quantum state $\mathbf{q} = (v, j, n, m)$ reads

$$P_R^X(\mathbf{q}) = \frac{\Sigma_R^X(\mathbf{a}, \mathbf{q})}{N_S + \Sigma_R^X(\mathbf{a})} \tag{17}$$

with

$$\Sigma_R^X(\mathbf{a}, \mathbf{q}) = \sum_{k=1}^{N-N_S} w_X(\mathbf{a})\ \delta_{x,v}\ \delta_{\bar{J}j}\ \delta_{a_n n}\ \delta_{a_m m}. \tag{18}$$

When the AC correction is applied, the expressions of the probabilities are unchanged, but $\Sigma_R^X(\mathbf{a})$ and $\Sigma_R^X(\mathbf{a}, \mathbf{q})$ are calculated only from non-adiabatic paths.

Results and discussion

A total of 200 energies were considered, spaced 2 meV apart on average, and 2 million trajectories were run at each energy. The Bulirsch-Stoer integrator was used, with an initial time step of 0.01 fs. ϵ was taken at 0.06 and 0.003 for the calculation of GB and 1GB weights, respectively. This ensures that the percentage of trajectories whose weights are larger than half their maximum possible value is close to 0.5 % for both GB and 1GB-QCT calculations. Their statistical efficiencies, or rate of convergence of the predictions in terms of number of trajectories run, are thus comparable.

For convenience's sake, we will call the quantum-corrected QCT calculations by the acronyms of the corrections (GB or 1GB, and AC whenever used). In the upper panel of Fig. 2, the GB and 1GB sticking probabilities (green triangles and red circles, respectively) are compared with the Q-TDWP one (black squares).

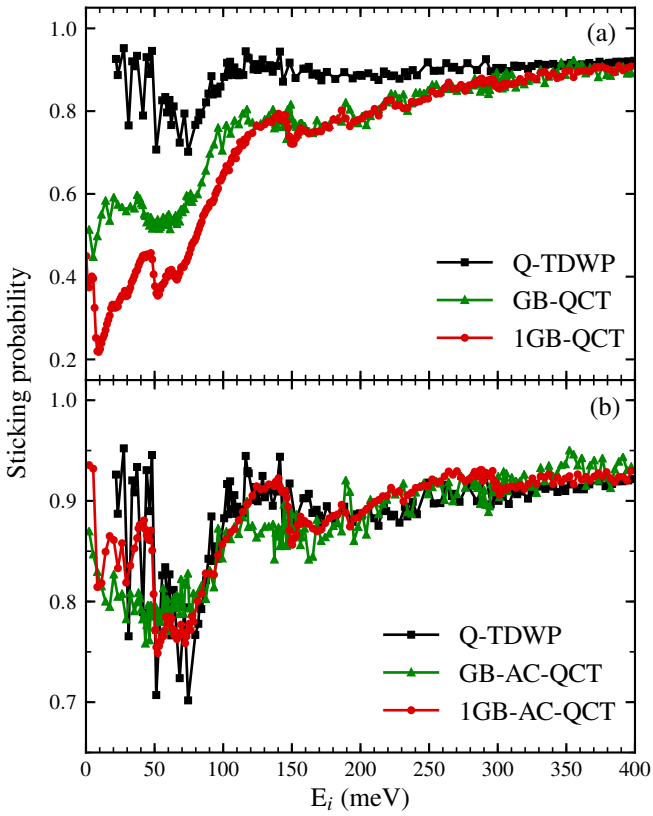

Figure 2: Collision energy dependence of the sticking probability for $H_2(0,0)$ + Pd(111) according to quantum calculations (black squares) and various quantum-corrected classical calculations involving GB, 1GB and AC (green triangles and red circles).

In contrast with the structureless SB probability (blue circles in Fig. 1), the GB and 1GB probabilities involve structures that resemble those present in the quantum probability, except that they are shifted downwards all the stronger as the collision energy is small. However, as shown in the lower panel of Fig. 2, the adiabaticity correction shifts upwards the GB and 1GB probabilities in such a way that the gap between the resulting GB-AC and 1GB-AC probabilities on one hand, and the quantum probability on the other hand, is dramatically reduced. This finding clearly illustrates the fact that the statistical weight carried by adiabatic paths is overestimated by the Gaussian binning procedures and that its redistribution among the remaining trajectories improves the predictions. In Fig. 3, the same comparison as previously is done for rovibrational state-resolved reflection probabilities. These are obtained by summing $P_R^{1GB}(\mathbf{q})$ (see Eq. 17) over Miller indices. The accuracy of 1GB-AC predictions is remarkable in the vicinity of thresholds (see panels (b) and (c)), and very satisfying elsewhere. Let us emphasize here that the probability of rovibrational excitation is a magnitude difficult to theoretically describe due to the high sensitivity of the final result to fine details of the interaction and dynamics.

A zoom on these probabilities around their respective thresholds is given in Fig. 4 for states (0,2) and (0,4). Moreover, the contributions of the five first diffraction orders to these probabilities are also shown. These contributions are obtained by summing $P_R^{1GB}(\mathbf{q})$ over those Miller indices corresponding to a given value of $E_\parallel(n,m)$ (see Eq. 8). For the zero order, the sum involves the single term $(n,m)=(0,0)$, and $E_\parallel(n,m)=0$; for the first order, the sum involves the six terms $(n,m)=(1,0)$, $(-1,0)$, $(0,1)$, $(0,-1)$, $(1,1)$ and $(-1,-1)$, and $E_\parallel(n,m)=8\pi^2/(3M\Delta^2)$. We do not enter into the details of higher orders. Their thresholds are indicated by vertical dash-dotted lines in Fig. 4. Note that each abrupt increase of these fully-resolved reflection probabilities is concomitent with the abrupt decrease of the sticking probability, as shown by a careful comparison between Fig. 4 and the black squares and red circles in Fig. 2.

In contrast, GB-AC reflection probabilities are only satisfying far from thresholds. In

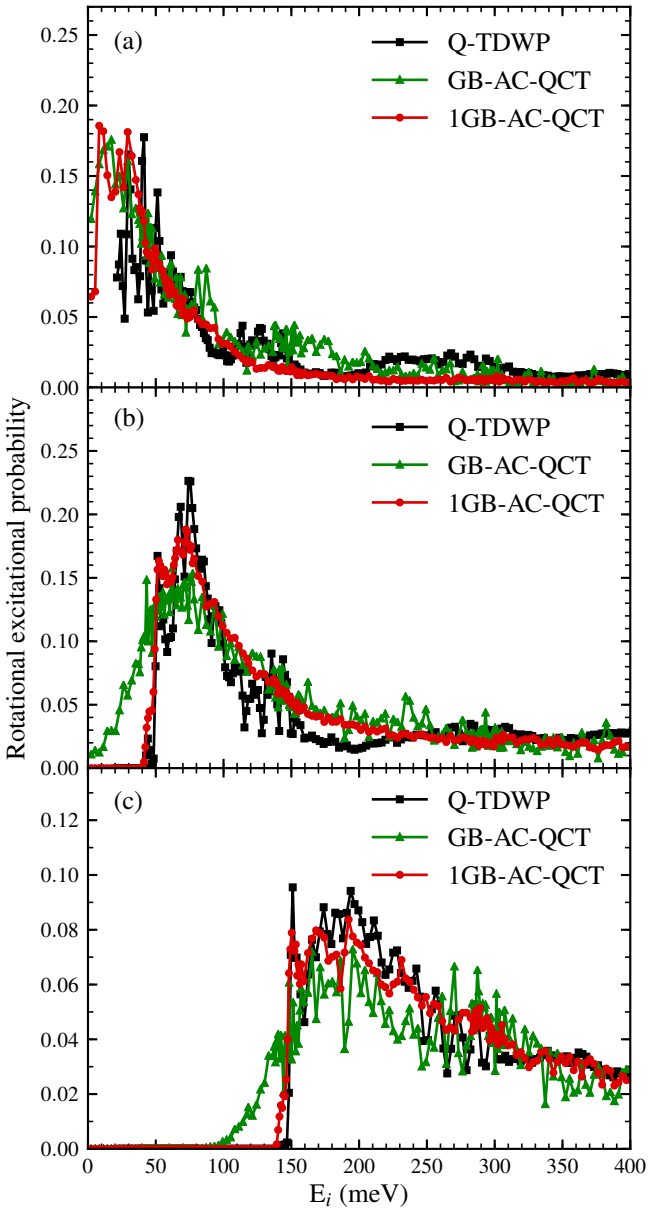

Figure 3: Collision energy dependence of rovibrationally elastic and inelastic scattering probabilities for H_2(0,0) + Pd(111) according to quantum calculations (black squares) and various quantum-corrected classical calculations involving GB, 1GB and AC (green triangles and red circles); Final state $(v, j) = (0, 0)$ (a), $(0, 2)$ (b), and $(0, 4)$ (c).

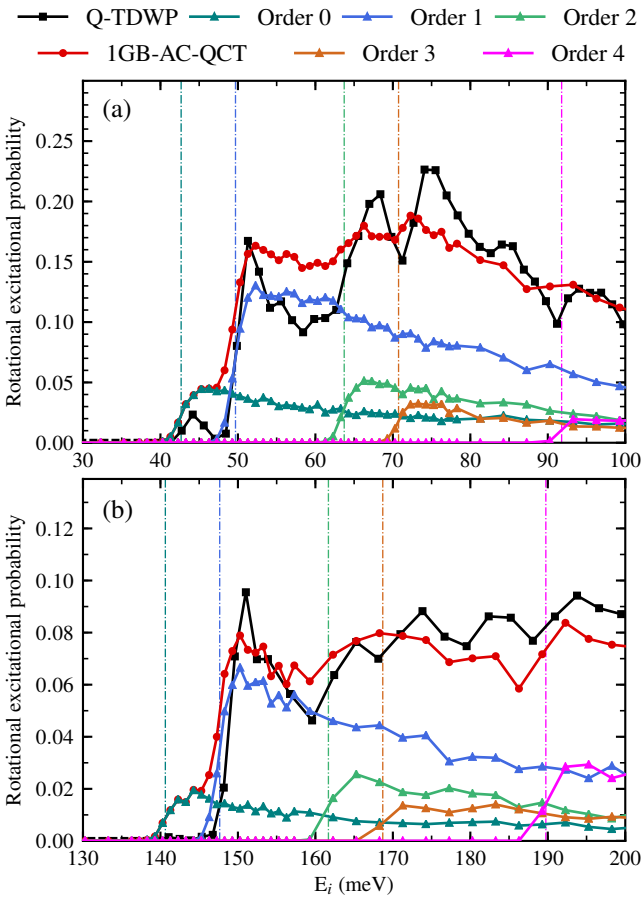

Figure 4: 1GB reflection probabilities for (v, j)=(0,2) (panel(a)) and (0,4) (panel (b)) in terms of the order of diffraction for the five first orders (see text for the definition of an order).

order to explain why, we ignore the quantization of the diffractive actions and use the rigid-rotor-harmonic-oscillator approximation so as to simplify the system.

The intrinsically quantized part of the energy, then, reduces to

$$E(\mathbf{a}) = \omega(x + \frac{1}{2}) + \frac{J(J+1)}{2Mr_e^2}. \tag{19}$$

ω is the vibrational frequency of H_2 and r_e its equilibrium bond length. The maximum value of $E(\mathbf{a})$ is given by

$$E(\mathbf{a}) = E_i + \frac{\omega}{2}, \tag{20}$$

where the right-hand-side is the total energy available to the final H_2. The points satisfying this identity form the upper bound of the available area in the (x, J) plane. In panels (a) and (b) of Fig. 5, this frontier is represented in the unit square associated with quantum state (0,2) for three values of E_i. The available area is located on the left side of the frontier. At E_i^a, (0,2) is not available. E_i^b corresponds to its opening. E_i^c is the symmetric of E_i^a with respect to E_i^b. Contour plot representations of the GB and 1GB weights, respectively given by Eq. 12 and 14, are also displayed. Integrating them over the region where they are larger than half their maximum possible value leads to 0.5 % in both cases (as for the calculations previously presented). Hence, their statistical efficiencies are equal. In panel (c), the integrals of the GB and 1GB weights obtained assuming a uniform distribution of the actions on the left side of the frontier are represented in terms of E_i. As a matter of fact, the sudden jump previously evoked appears to be described far better by the 1GB procedure than by the GB one, as expected from the contour levels in the upper panels.

Conclusions

In this work, we have performed, for the first time, the pseudo-quantization in Bohr's spirit of all the relevant final actions of a classically described reactive molecular system. The

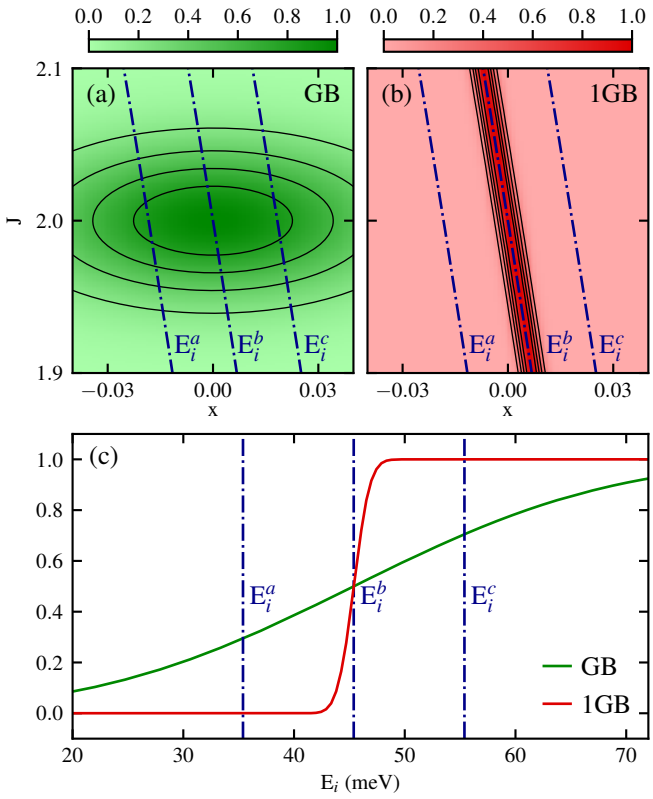

Figure 5: Rescaled GB and 1GB weights are represented in panels (a) and (b), respectively. Blue lines correspond to three different collision energies E_i^a, E_i^b and E_i^c whose values can be guessed from panel (c). E_i^b is the energy of state (0,2). The domains of the (x, J) space available at these energies are located on the left side of the blue lines in panels (a) and (b). Integrating the GB and 1GB weights assuming a uniform distribution in the available domain at E_i leads to the green and red curves in panel (c), respectively. The sudden jump observed with 1GB shows the suitability of this procedure to realistically describe energy thresholds.

process at hand is the scattering of H_2 on Pd(111), and the final actions are the vibrational and rotational actions of the reflected H_2 diatom, as well as the diffractive actions (classical analogs of Miller indices). The pseudo-quantization was ensured by means of both action-based Gaussian binning (GB) and energy-based Gaussian binning (1GB), the latter being commonly employed for polyatomic reactions since a decade ago.[16,45] Importantly, we have adjusted Gaussian widths so as to give to both procedures the same statistical efficiency. In addition to that, we have used the adiabaticity correction (AC).[32]

The major result of this study is that 1GB-AC quasi-classical trajectory (QCT) calculations lead to a spectacular agreement with state-of-the-art quantum scattering results (sticking and state-resolved reflection probabilities). To the best of our knowledge, this method improves on any previous quasi-classical description.

It is planned to repeat this study for different gas-phase and gas-surface reactions in order to figure out whether the quality of the present agreement between quantum corrected QCT and exact quantum probabilities is systematically maintained or not. If it is indeed confirmed that the accuracy is equally good for a large variety of systems and dynamical situations, the current methodology can be a reliable alternative to computationally heavy quantum dynamics calculations. It may be also applicable to systems of increasing complexity and/or energy regimes not currently accessible in quantum dynamics, such as low incident energies.

Last but not least, it will be desirable to keep strengthening the theoretical grounds of the quantum corrections (GB, 1GB and AC) within the framework of the semiclassical description of molecular processes.

Acknowledgement

A.R.F. acknowledges financial support by the University of Bordeaux. The authors acknowledge the support of France Grilles for providing computing resources on the French National Grid Infrastructure. Computer time was provided as well by the Pôle Modélisation HPC

facilities of the Institut des Sciences Moléculaires UMR 5255 CNRS Université de Bordeaux, co-funded by the Nouvelle Aquitaine region as well as the MCIA (Mésocentre de Calcul Intensif Aquitain) resources of the Université de Bordeaux and of the Université de Pau et des Pays de l'Adour. The authors acknowledge financial support by the Spanish Ministerio de Economia, Industria y Competitividad Grant No. FIS2016-76471-P. This work was conducted in the scope of the transborder joint Laboratory "QuantumChemPhys: Theoretical Chemistry and Physics at the Quantum Scale (ANR-10-IDEX-03-02)."

Supporting Information Available

The Supporting Information contains detailed information about the diffractive actions.

This material is available free of charge via the Internet at `http://pubs.acs.org/`.

References

(1) Kroes, G.-J.; Díaz, C. Quantum and Classical Dynamics of Reactive Scattering of H2 from Metal Surfaces. *Chem. Soc. Rev.* **2016**, *45*, 3658.

(2) H., G.; Liu, K. Control of Chemical Reactivity by Transition-State and Beyond. *Chem. Sci.* **2016**, *7*, 3992.

(3) Wodtke, A. M. Electronically Non-Adiabatic Influences in Surface Chemistry and Dynamics. *Chem. Soc. Rev.* **2016**, *45*, 3641.

(4) Golibrzuch, K.; Bartels, N.; Auerbach, D. J.; Wodtke, A. M. The Dynamics of Molecular Interactions and Chemical Reactions at Metal Surfaces: Testing the Foundations of Theory. *Annu. Rev. Phys. Chem.* **2015**, *66*, 399.

(5) Yang, X.; Clary, D. C.; Neumark, M. Chemical Reaction Dynamics. *Chem. Soc. Rev.* **2017**, *46*, 7481.

(6) Nichols, B.; Chadwick, H.; Gordon, S. D. S.; Eyles, C. J.; Hornung, B.; Brouard, M.; Alexander, M. H.; Aoiz, F. J.; Gijsbertsend, A.; Stolte, S. Steric effects and quantum interference in the inelastic scattering of NO(X) + Ar. *Chem. Sci.* **2015**, *6*, 2202.

(7) Díaz, C.; Pijper, E.; Olsen, R. A.; Busnengo, H. F.; Auerbach, D. J.; Kroes, G.-J. Chemically Accurate Simulation of a Prototypical Surface Reaction: H2 Dissociation on Cu(111). *Science* **2009**, *316*, 832.

(8) Pan, H.; Liu, K.; Caracciolo, A.; Casavecchia, P. Crossed beam polyatomic reaction dynamics: recent advances and new insights. *Chem. Soc. Rev.* **2017**, *46*, 7517.

(9) Bonnet, L.; Espinosa-Garcia, J. Simulation of the experimental imaging results for the OH + CHD_3 reaction with a simple and accurate theoretical approach. *Phys. Chem. Chem. Phys.* **2017**, *19*, 20267.

(10) Alducin, M.; Muino, R. D.; Juaristi, J. I. Non-adiabatic effects in elementary reaction processes at metal surfaces. *Prog. Surf. Sci.* **2017**, *92*, 317.

(11) Zhang, D. H.; Guo, H. Recent Advances in Quantum Dynamics of Bimolecular Reactions. *Annu. Rev. Phys. Chem.* **2016**, *67*, 135.

(12) Fu, B.; Shan, X.; Zhang, D. H.; Clary, D. C. Recent Advances in Quantum Scattering Calculations on Polyatomic Bimolecular Reactions. *Chem. Soc. Rev.* **2017**, *46*, 7625.

(13) Pan, H.; Liu, K.; Caracciolo, A.; Casavecchia, P. Crossed beam polyatomic reaction dynamics: recent advances and new insights. *Chem. Soc. Rev.* **2017**, *46*, 7517.

(14) Nattino, F.; Migliorini, D.; Kroes, G.-J.; Dombrowski, E.; High, E. A.; Killelea, D. R.; Utz, A. L. Chemically Accurate Simulation of a Polyatomic Molecule-Metal Surface Reaction. *J. Phys. Chem. Lett.* **2016**, *7*, 2402, PMID: 27284787.

(15) Braunstein, M.; Conforti, P. Classical Dynamics of H_2O Vibrational Self-Relaxation. *J. Phys. Chem. A* **2015**, *119*, 3311.

(16) Czakó, G.; Bowman, J. M. Quasiclassical trajectory calculations of correlated product distributions for the F+CHD3(v1=0,1) reactions using an ab initio potential energy surface. *J.Chem. Phys.* **2009**, *131*, 244302.

(17) Matsugi, A. Dissociation channels, collisional energy transfer, and multichannel coupling effects in the thermal decomposition of CH3F. *Phys. Chem. Chem. Phys.* **2018**, *20*, 15128.

(18) Ping, L.; Tian, L.; Song, H.; Yang, M. New Method To Extract Final-State Information of Polyatomic Reactions Based on Normal Mode Analysis. *J. Phys. Chem. A* **2018**, *122*, 6997.

(19) Vázquez, S. A.; Otero, X. L.; Martinez-Nunez, E. A Trajectory-based method to explore reaction mechanisms. *Molecules* **2018**, *23*, 3156.

(20) Espinosa-Garcia, J.; Garcia-Chamorro, M. Role of an ethyl radical and the problem of HF(v) bimodal vibrational distribution in the $F(^2P) + C_2H_6 \longrightarrow HF(v) + C_2H_5$ reaction. *Phys. Chem. Chem. Phys.* **2018**, *20*, 26634.

(21) Corchado, J. C.; Chamorro, M. G.; Rangel, C.; Espinosa-Garcia, J. State-to-state dynamics of the $Cl(^2P) + C_2H_6(\nu_5, \nu_1 = 0, 1) \longrightarrow HF(v) + C_2H_5$ hydrogen abstraction reactions. *Theor. Chem. Acc.* **2019**, *138:26*.

(22) Shao, K.; Fu, B.; Zhang, D. H. A global full-dimensional potential energy surface and quasiclassical trajectory study of the $O(^1D) + CH_4$ multichannel reaction. *Phys. Chem. Chem. Phys.* **2015**, *17*, 24098.

(23) Guo, H.; Farjamnia, A.; Jackson, B. Effects of Lattice Motion on Dissociative Chemisorption: Toward a Rigorous Comparison of Theory with Molecular Beam Experiments. *J. Phys. Chem. Lett.* **2016**, *7*, 22.

(24) Bonnet, L.; Linguerri, R.; Hochlaf, M.; Yazidi, O.; Halvick, P.; Francisco, J. S. Full-Dimensional Theory of Pair-Correlated HNCO Photofragmentation. *J. Phys. Chem. Lett.* **2017**, *8*, 2420.

(25) Macaluso, V.; Homayoon, Z.; Spezia, R.; Hase, W. L. Threshold for shattering fragmentation in collision-induced dissociation of the doubly protonated tripeptide $TIK(H^+)_2$. *Phys. Chem. Chem. Phys.* **2018**, *20*, 19744.

(26) Roncero, O.; Zanchet, A.; Aguado, A. Low temperature reaction dynamics for CH_3OH + OH collisions on a new full dimensional potential energy surface. *Phys. Chem. Chem. Phys.* **2018**, *20*, 25951.

(27) Nagy, T.; Lendvay, G. Adiabatic Switching Extended To Prepare Semiclassically Quantized RotationalâĹŠVibrational Initial States for Quasiclassical Trajectory Calculations. *J. Phys. Chem. Lett.* **2017**, *8*, 4621.

(28) Kasai, T.; Che, D.; Tsai, P.; Nakamura, M.; Muthiah, B.; Lin, K.-C. Roaming and chaotic behaviors in collisional and photoâĂŘinitiated molecularâĂŘbeam reactions: a role of classical vs. quantum nonadiabatic dynamics. *Rendiconti Lincei, Scienze Fisiche e Naturali* **2018**, *29*, 219.

(29) Bonnet, L. Classical Dynamics of Chemical Reactions in a Quantum Spirit. *Int. Rev. Phys. Chem.* **2013**, *32*, 171.

(30) Bonnet, L.; Rayez, J. Quasiclassical trajectory method for molecular scattering processes: necessity of a weighted binning approach. *Chem. Phys. Lett.* **1997**, *277*, 183.

(31) Bonnet, L.; Rayez, J.-C. Gaussian weighting in the quasiclassical trajectory method. *Chem. Phys. Lett.* **2004**, *397*, 106.

(32) Bonnet, L. The method of Gaussian weighted trajectories. III. An adiabaticity correction proposal. *J. Chem. Phys.* **2008**, *128*, 044109.

(33) Crespos, C.; Decock, J.; Larrégaray, P.; Bonnet, L. Classical MoleculeâĂŞSurface Scattering in a Quantum Spirit: Application to H2/Pd(111) Nonactivated Sticking. *J. Phys. Chem. C* **2017**, *121*, 16854.

(34) Lara, M.; Chefdeville, S.; Larregaray, P.; Bonnet, L.; Launay, J.-M.; Costes, M.; Naulin, C.; Bergeat, A. S(^{1}D) + ortho-D_2 Reaction Dynamics at Low Collision Energies: Complementary Crossed Molecular Beam Experiments and Theoretical Investigations. *J. Phys. Chem. A* **2016**, *120*, 5274.

(35) Díaz, C.; Busnengo, H. F.; Rivière, P.; Farías, D.; Nieto, P.; Somers, M. F.; Kroes, G. J.; Salin, A.; Martín, F. A classical dynamics method for H2 diffraction from metal surfaces. *J. Chem. Phys.* **2005**, *122*, 154706.

(36) C. Díaz, C.; Somers, M. F.; Kroes, G.-J.; Busnengo, H. F.; Salin, A.; Martin, F. *Phys. Rev. B* **2005**, *72*, 035401.

(37) Farias, D.; Diaz, C.; Nieto, P.; Salin, A.; Martin, F. Pronounced out-of-plane diffraction of H2 molecules from a Pd(1 1 1) surface. *Chem. Phys. Lett.* **2004**, *390*, 250.

(38) Resh, C.; Berger, H. F.; Rendulic, K. D. *Surf. Sci.* **1994**, *L1105*, 316.

(39) Resh, C.; Berger, H. F.; Rendulic, K. D. *Chem. Phys. Lett.* **1995**, *247*, 249.

(40) Busnengo, H.; Pijper, E.; Somers, M.; Kroes, G.; Salin, A.; Olsen, R.; Lemoine, D.; Dong, W. Six-dimensional quantum and classical dynamics study of H2($\hat{I}_i$=0,J=0) scattering from Pd(111). *Chem. Phys. Lett.* **2002**, *356*, 515.

(41) Busnengo, H. F.; Crespos, C.; Dong, W.; Rayez, J. C.; Salin, A. Classical dynamics of dissociative adsorption for a nonactivated system: The role of zero point energy. *J.Chem. Phys.* **2002**, *116*, 9005.

(42) Dong, W.; Hafner, J. H_2 dissociative adsorption on Pd(111). *Phys. Rev. B* **1997**, *56*, 15396.

(43) Child, M. S. *Semiclassical Mechanics with Molecular Applications*; Oxford University Press, USA, 1991.

(44) Bradley, K. S.; Schatz, G. C. A Quasiclassical Trajectory Study of Product Energy and Angular Distributions in OH + H2 (D2). *The Journal of Physical Chemistry* **1994**, *98*, 3788.

(45) Bonnet, L.; Espinosa-García, J. The method of Gaussian weighted trajectories. V. On the 1GB procedure for polyatomic processes. *J.Chem. Phys.* **2010**, *133*, 164108.